HHS Public Access

Author manuscript

Science. Author manuscript; available in PMC 2017 September 30.

Published in final edited form as:

Science. 2017 March 31; 355(6332): 1411–1415. doi:10.1126/science.aai7984.

Breathing Control Center Neurons that Promote Arousal in Mice

Kevin Yackle[1,#], **Lindsay A. Schwarz**[2], **Kaiwen Kam**[3,4], **Jordan M. Sorokin**[5], **John R. Huguenard**[5], **Jack L. Feldman**[3], **Liqun Luo**[2], and **Mark A. Krasnow**[1,*]

[1]Howard Hughes Medical Institute, Department of Biochemistry, Stanford University School of Medicine, Stanford CA 94305, U.S.A

[2]Howard Hughes Medical Institute, Department of Biology, Stanford University, Stanford CA 94305, U.S.A

[3]Systems Neurobiology Laboratory, Department of Neurobiology, David Geffen School of Medicine, University of California Los Angeles, Los Angeles, CA 90095, U.S.A

[4]Department of Cell Biology and Anatomy, Chicago Medical School, Rosalind Franklin University of Medicine and Science, North Chicago, IL, 60064, U.S.A

[5]Department of Neurology and Neurological Sciences, Stanford University, Stanford CA 94305, U.S.A

Abstract

Slow, controlled breathing has been used for centuries to promote mental calming, and it is used clinically to suppress excessive arousal such as panic attacks. However, the physiological and neural basis of the relationship between breathing and higher order brain activity is unknown. We found a neuronal subpopulation in the mouse preBötzinger Complex (preBötC), the primary breathing rhythm generator, which regulates the balance between calm and arousal behaviors. Conditional, bilateral genetic ablation of the ~175 *Cdh9/Dbx1* double-positive preBötC neurons in adult mice left breathing intact but increased calm behaviors, and decreased time in aroused states. These neurons project to, synapse on, and positively regulate noradrenergic neurons in the locus coeruleus, a brain center implicated in attention, arousal and panic that projects throughout the brain.

*Corresponding author: krasnow@stanford.edu.
#Current address: Department of Physiology, University of California San Francisco, San Francisco, CA 94158

Supplementary Materials
Materials and Methods
Figs. S1–15
Table S1
Movie S1
References (29–46)

K.Y. performed *in situ* screen, generated and characterized Cdh9 transgene, characterized Cdh9/Dbx1 neuronal ablation, performed AAV-Cre, Fluorogold, and retrograde bead injections, and c-Fos experiments. L.A.S. and L.L. provided reagents for and L.A.S. injected rabies and CAV-Cre viruses. K.K. and J.L.F. provided reagents for and K.K. performed and analyzed slice electrophysiology. J.M.S. and J.R.H. provided reagents for and J. M.S. performed and analyzed ECoG recording. K.Y. analyzed all data. K.Y. and M.A.K. conceived experiments, interpreted data and wrote the manuscript. All authors edited the manuscript.

Data is curated and stored in the Krasnow lab: Howard Hughes Medical Institute, Department of Biochemistry, Stanford University School of Medicine, Stanford CA 94305, U.S.A

Although breathing is commonly viewed as a simple autonomous function that sustains life, it has long been known to influence higher order behavior and thinking (1). Slow controlled breathing is used by practitioners of pranayama yoga and other forms of meditation to promote mental calming and contemplative states, and it is used clinically to suppress excessive arousal and stress such as certain types of panic attacks (2,3). While the effect of breathing on behavior and mental state could easily be indirect, there could also be more direct connections and impact of the breathing center on higher order brain function (4), as demonstrated here.

The preBötzinger Complex (preBötC) is a cluster of several thousand neurons in the ventrolateral medulla of the murine brain that can autonomously generate respiratory rhythms in explanted brain slices (5, 6), and whose rhythmic activity in vivo initiates breathing by recurrently activating pre-motor and motor neurons of the respiratory muscles (5). The preBötC is not a homogenous population of neurons but is composed of distinct though intermingled neuronal subpopulations (5, 7), one of which is essential for respiratory rhythm generation (8, 9) and another for sighing (10).

To systematically explore the molecular diversity of breathing center neurons, we screened expression patterns of over 19,000 genes in the Euroexpress e14.5 mouse hindbrain database (7, 11). Cadherin-9 (Cdh9) was the gene most selectively expressed in preBötC (Fig. 1A). We constructed a bacterial artificial chromosome (BAC) transgene with mOrange coding sequence inserted at the Cdh9 translation start codon (Fig. 1B). Cell counts in early postnatal brains detected 319 ± 130 (n = 6) Cdh9-mOrange expressing cells in preBötC (Fig. 1C). These cells intermingled with neurons expressing canonical preBötC markers Somatostatin (SST) and Neurokinin 1 receptor (NK1R) (Fig. 1D to E, and fig. S1A–E). Few expressed the markers themselves: 0 of 43 Cdh9+ cells scored were SST+, and 7 of 179 Cdh9+ cells scored (4%) were NK1R+. All Cdh9-mOrange expressing cells co-expressed neuronal marker NeuN (n = 61 cells, Fig. 1F). These Cdh9-mOrange-expressing neurons can be further divided into seven subtypes based on differential expression of transcription factors PAX2, DACH1, LMO4, EVX1 and Dbx1 (7). We focused on the ~175 neurons in each preBötC (fig. S1F–J; ~350 neurons bilaterally) that co-express the Dbx1 lineage marker, the major subpopulation (56%, 165 of 292 scored Cdh9+ cells, were Dbx1-LacZ+) we call Cdh9/Dbx1 neurons (Fig. 1G to I).

We electrophysiologically recorded 26 mOrange-positive neurons in 15 preBötC slice preparations from Cdh9-mOrange;Dbx1-lacZ double transgenic P0–5 mice, then post-stained for beta-galactosidase (lacZ) in some preparations to identify recordings of Cdh9/Dbx1 neurons (Table S1). We definitively identified five Cdh9/Dbx1 neurons. One showed bursts of action potentials just before or during each preBötC inspiratory burst (Fig. 1J, and fig. S2), like most other Dbx1 lineage preBötC neurons (12). Three other neurons were more broadly active with bursts during some but not all preBötC inspiratory bursts (42, 41, and 88% of inspiratory bursts, Fig. 1K, and fig. S2), called an “inspiratory-associated” activity pattern. The other neuron showed sporadic activity with no apparent relationship to preBötC inspiratory bursts. Seven of the 15 Cdh9-mOrange neurons whose Dbx1-lacZ expression status was not determined also displayed inspiratory (4 neurons) or inspiratory-associated (2 neurons) patterns (Table S1).

We used intersectional genetics (Cdh9-LOSL-DTR;Dbx1-Cre) (Fig. 1B,M,N) to express human diphtheria toxin receptor (DTR) only in Dbx1 lineage cells that co-express Cdh9, so that Cdh9/Dbx1 neurons could be specifically ablated by intraperitoneal injection of diphtheria toxin. We expected there would be few if any cells besides Cdh9/Dbx1 preBötC neurons that express both genes (11, 13). We examined this in two ways. First, we compared mOrange expression in Cdh9-LOSL-DTR and Cdh9-LOSL-DTR;Dbx1-Cre transgenic mice by immunostaining serial sections of adult brains. The only regions where Dbx1-Cre reduced the number of mOrange-expressing cells were preBötC and inferior colliculus (fig. S3). Co-staining with other markers showed that loss of mOrange in preBötC was specific and complete for Cdh9/Dbx1 neurons and had little or no effect on the six other (Dbx1-negative) Cdh9-positive preBötC cell types (fig. S4). Second, immunostaining of serial sections of Cdh9-LOSL-DTR;Dbx1-Cre adult brains detected DTR expression only in preBötC Cdh9/Dbx1 neurons (Fig. 1M) and the inferior colliculus (fig. S3). Intraperitoneal injection of diphtheria toxin once a day for three days eliminated the DTR-expressing cells (Fig. 1N).

We analyzed adult mice several days after ablating Cdh9/Dbx1 neurons. We expected Cdh9/Dbx1 neurons would be essential for breathing and viability because Dbx1 neurons are essential for breathing in vivo (8, 9), and ablating just 85 random Dbx1 neurons abolishes preBötC rhythms in vitro (14). However, there was no overt effect on viability (3 of 3 scored mice alive >1 year post ablation), breathing, or on sensory and motor behaviors. Plethysmography of freely moving adult mice after ablation did not detect significant differences in inspiratory time, expiratory time or tidal volume of standard (eupneic) breaths (figs. S5A,S6). No differences were detected in characteristics of four variant breath types (fig. S5B to E, S6) or breaths during sleep or under hypercapnic or hypoxic conditions (figs. S5F to H, S6).

There was, however, a change in abundance of different breath types, first noted in respiratory rate (RR) histograms: Cdh9/Dbx1 ablation shifted the distribution toward slower breaths (low RR) (Fig. 2B). Inspection of plethysmograph traces indicated that the shift was due to increased slow breaths (eupneic and grooming) associated with calm behaviors, and reduction in rapid breaths associated with sniffing and other active behaviors (Fig. 2A, and fig. S7).

The change in breathing patterns after Cdh9/Dbx1 neural ablation was accompanied by a corresponding change in behavior. Ablation reduced exploration of a new environment (87% ± 9% vs. 62% ± 20% time spent in active exploration, pre- vs. post-ablation; p=0.02) and increased time engaged in grooming three-fold (10% ± 7% vs. 31% ± 16%; p = 0.02) and still sitting twofold (3% ± 4% vs. 7% ± 7%; p = 0.07), although the latter did not reach statistical significance (Fig. 2C). There was an increase in both number of calm episodes (Fig. 2D) and their duration (Fig. 2E, and movie S1). Because the breathing pattern associated with each behavioral state was not detectably altered by ablation (figs. S5,S6), the observed change in RR distribution could be explained by the overall change in behavior (fig. S8): a shift from active toward calm behaviors. Electrocorticographic (ECoG) monitoring showed an increase in slow wave (delta, 2–4Hz) brain activity after ablation (Fig. 2F), and a selective decline in time spent in an active brain state dominated by theta activity

(Fig. 2G) compared to littermate controls (Fig. 2H, I). These changes could be temporarily reversed by illuminating the chamber, providing a stimulus that apparently overrides the decrease in arousal caused by Cdh9/Dbx1ablation (fig. S9).

To confirm that the observed behavioral and breathing changes were due to ablation of neurons within the preBötC, we restricted DTR induction and hence neural ablation to just Cdh9-expressing preBötC neurons (fig. S10A–C). The animals displayed a diminution in active exploratory behaviors and breathing patterns and increase in calm behaviors and breathing patterns similar to animals with Cdh9/Dbx1 neurons ablated using our intersectional genetic strategy (compare fig. S10D,E and Fig. 2).

The decrease in active behavior and increase in ECoG delta waves observed after Cdh9/Dbx1 neuron ablation is reminiscent of changes following silencing or ablation of the locus coeruleus (LC), a noradrenergic nucleus in the pons implicated in generalized arousal, stress, and sleep-wake transitions (15). We thus microinjected two retrograde tracers into the LC and found that both labeled Cdh9-mOrange neurons in preBötC (FluorGold: fig. S11A to C; fluorescent retrograde beads: data not shown). Most of the labeled Cdh9-mOrange preBötC neurons (85%, 23/27, n = 40 sections, 3 mice) were contralateral to the injection site. The connection is selective because most labeled preBötC neurons expressed Cdh9-mOrange (72%, 13/18, n = 10 sections, 4 mice), and no retrograde labeling of Cdh9-mOrange neurons was observed following tracer injection into regions surrounding the LC (n = 4 injections).

We tested whether the observed connection between the preBötC neurons and LC is direct to the noradrenergic (dopamine beta hydroxylase (Dbh)-expressing) neurons that dominate the LC (15). Injection of Cre-dependent AAV helper viruses (AAV-FLExLoxP-TVA:mCherry and AAV-FLExLoxP-rabies glycoprotein), which enables infection and monosynaptic spread of an envA-pseudotyped, glycoprotein-deleted, and GFP-expressing rabies virus (RVdG) (16), into the LC of Dbh-Cre;Cdh9-mOrange mice resulted in specific infection of LC “starter” neurons by RVdG (fig. S12) and selective retrograde trans-synaptic tracing (GFP-labeling) of Cdh9-mOrange neurons in the preBötC (Fig. 3A to D and fig. S11D to F). We again observed a strong bias for labeling the contralateral rather than ipsilateral preBötC (compare Fig. 3A to C and fig. S11D to F). Most of the GFP-labeled neurons in the contralateral preBötC (63%, 45/72, n = 18 sections, 3 mice) expressed Cdh9-mOrange, whereas few of the labeled ipsilateral preBötC neurons expressed Cdh9-mOrange (7%, 7/94, n = 18 sections,3 mice). Nearly all ipsilateral GFP-expressing neurons were located outside the canonical preBötC region defined by Somatostatin expression, so they are presumably not preBötC neurons (fig. S13). Control experiments in mice without Dbh-Cre did not show double-positive preBötC neurons (fig. S12).

We microinjected a retrogradely-transported Cre-expressing virus, Canine Adenovirus Type 2-Cre (CAV-Cre), bilaterally into the LC of Cdh9-LOSL-DTR mice to eliminate mOrange and express DTR only in the Cdh9-expressing neurons that project to LC (Fig. 3E). Before DT injection, animals breathed and behaved normally, although there was an increase in calm breathing relative to mock-ablated controls, perhaps because of neural toxicity associated with induced DTR expression (Fig. 3H and I). 4–10 days after DT injection and ablation of LC-projecting, Cdh9-expressing preBötC neurons (Fig. 3F,G), there was a

change in breathing (Fig. 3H) and decrease in active behaviors (Fig. 3I) that mimicked those observed after ablation of the Cdh9/Dbx1 preBötC neurons (compare to Fig. 2B and C).

We examined LC activity by c-FOS expression (17) following Cdh9/Dbx1 neuron ablation. Under standard housing conditions, Cdh9-LOSL-DTR;Dbx1-Cre littermate control mice with intact Cdh9/Dbx1 neurons showed occasional LC activity (Fig. 4A and D, and fig. S14). When animals were placed in a new environment (plethysmography chamber) for 1 hour, c-FOS was induced in scattered cells throughout the LC (Fig. 4B and D, and fig. S14). However, four days after Cdh9/Dbx1 neuron ablation, only rare c-FOS positive LC neurons were detected before or after placement in the chamber (Fig. 4C and D, and fig. S14). The LC of ablated animals remained responsive to the extreme arousal stimulus of physical restraint stress (18) (Fig. 4D to F, and fig. S13), indicating that other LC inputs and functions were intact.

We have identified and characterized a new neuronal subtype in the preBötC comprising ~175 of its ~3000 neurons. The Cdh9/Dbx1are dispensable for respiratory rhythm generation and instead promote generalized behavioral arousal. Ablation of these neurons left all major breathing patterns and regulation intact, but made the mice preternaturally calm: their activity and ECoG profiles shifted from active exploratory behavior and brain wave patterns toward calm behaviors such as still sitting and grooming. Monosynaptic tracing demonstrated that these neurons directly project to and synapse on noradrenergic neurons in the contralateral LC, which in turn project throughout the brain and control generalized arousal and sleep-wake transitions (15). preBötC Cdh9/Dbx1 neurons provide excitatory input to the LC, and appear to be the dominant activating input under mild arousal conditions of placement in a new chamber.

We propose that Cdh9/Dbx1 preBötC neurons function as gateway neurons directly linking the preBötC to the locus coeruleus, and through it to the rest of the brain (Fig. 4G). This ascending circuit allows the respiratory center to communicate directly with and control higher order brain structures associated with behavioral arousal. The excitatory input to the LC is presumably provided by the observed inspiratory-associated activity patterns of Cdh9/Dbx1 neurons, which could provide greater excitatory input with faster respiratory rates and perhaps abnormal respiratory patterns (Fig. 4H). This respiratory corollary signal would thus serve to coordinate the animal's state of arousal with the breathing pattern, leaving the animal calm and relaxed when breathing is slow and regular, but promoting (or maintaining) arousal when breathing is rapid or disturbed. This circuit and corollary signal would explain why preBötC respiratory patterns have been observed in the LC and other reticular activating structures (19–21). The LC can increase respiratory rate (22), so there may also be a positive feedback loop from the LC ultimately back to Cdh9/Dbx1 preBötC neurons.

The Cdh9/Dbx1 circuit may have evolved as a direct and rapid defense response, mobilizing the animal in the face of rapid, irregular or labored breathing. Indeed, fast or erratic breathing in humans increases alertness and can cause anxiety and even panic (3), and likewise increased preBötC activity, hyperventilation, and sighs appear to induce arousal during sleep (23–25). Conversely, slow and controlled breathing have long been known by practitioners of pranayama yoga to induce relaxation, and related approaches have proven

useful in anxiety syndromes and other stress disorders (1, 2). If the Cdh9/Dbx1 circuit is conserved in humans, it could provide a therapeutic target for breathing-related anxiety disorders and perhaps prevention of sudden infant death syndrome (SIDS), widely hypothesized to result from inadequate arousal response to asphyxiation during sleep (24). Interestingly, panic attacks triggered by respiratory symptoms are uniquely responsive to clonidine, an α2-adrenergic agonist that silences LC (26).

Although breathing is generally thought of as an autonomic behavior, higher order brain functions can exert exquisite control over breathing. Our results show, conversely, that the breathing center has a direct and powerful influence on higher order brain function. It will thus be important to map the full range of behaviors and functions the breathing center controls.

Supplementary Material

Refer to Web version on PubMed Central for supplementary material.

Acknowledgments

We thank Drs. Xiaoke Chen and Greg Nachtrab for assistance and reagents for AAV-Cre injection, Jamie Zeitzer for assistance with ECoG analysis, and members of the Krasnow lab for helpful comments. This work was supported by the Howard Hughes Medical Institute (M.A.K. and L.L.), NIH grants HL70029 (J.L.F.), HL40959 (J.L.F.) and the NIH Medical Scientist Training Program (K.Y.). M.A.K. and L.L. are investigators of the Howard Hughes Medical Institute.

References and Notes

1. Brown RP, Gerbarg PL. Yoga breathing, meditation, and longevity. Ann N Y Acad Sci. 2009; 1172:54–62. [PubMed: 19735239]
2. Brown RP, Gerbarg PL. Sudarshan Kriya Yogic breathing in the treatment of stress, anxiety, and depression: part II-clinical applications and guidelines. J Altern Complement Med. 2005; 11:711–717. [PubMed: 16131297]
3. Nardi E, Freire RC, Zin WA. Panic disorder and control of breathing. Respir Physiol Neurobiol. 2009; 167:133–143. [PubMed: 18707030]
4. Parshall MB, et al. An official american thoracic society statement: update on the mechanisms, assessment, and management of dyspnea. Am J of Respir Crit Care Med. 2012; 185:435–452. [PubMed: 22336677]
5. Feldman JL, Del Negro CA, Gray PA. Understanding the rhythm of breathing: so near, yet so far. Annu Rev Physiol. 2013; 75:423–452. [PubMed: 23121137]
6. Smith JC, Ellenberger HH, Ballanyi K, Richter DW, Feldman JL. Pre-Bötzinger complex: a brainstem region that may generate respiratory rhythm in mammals. Science. 1991; 254:726–729. [PubMed: 1683005]
7. Yackle K, Ezran C, Kam K, Krasnow MA. in preparation.
8. Bouvier J, et al. Hindbrain interneurons and axon guidance signaling critical for breathing. Nature Neuroscience. 2010; 13:1066–1074. [PubMed: 20680010]
9. Gray PA, et al. Developmental origin of preBotzinger complex respiratory neurons. J Neurosci. 2010; 30:14883–14895. [PubMed: 21048147]
10. Li P, et al. The peptidergic control circuit for sighing. Nature. 2016; 530:293–297. [PubMed: 26855425]
11. Diez-Roux G, et al. A high-resolution anatomical atlas of the transcriptome in the mouse embryo. PLoS Biol. 2011; 9:e1000582. [PubMed: 21267068]

12. Picardo MC, Weragalaarachchi KT, Akins VT, Del Negro CA. Physiological and morphological properties of Dbx1-derived respiratory neurons in the pre-Bötzinger complex of neonatal mice. J Physiol. 2013; 591:2687–2703. [PubMed: 23459755]
13. Pierani A, Moran-Rivard L, Sunshine MJ, Littman DR, Goulding M, Jessell TM. Control of interneuron fate in the developing spinal cord by the progenitor homeodomain protein Dbx1. Neuron. 2001; 29:367–384. [PubMed: 11239429]
14. Wang X, et al. Laser ablation of Dbx1 neurons in the pre-Bötzinger complex stops inspiratory rhythm and impairs motor output in neonatal mice. eLife. 2014; 3:e03427. [PubMed: 25027440]
15. Berridge CW, Waterhouse BD. The locus coeruleus-noradrenergic system: modulation of behavioral state and state-dependent cognitive processes. Brain Res Brain Res Rev. 2003; 42:33–84. [PubMed: 12668290]
16. Wickersham R, et al. Monosynaptic restriction of transsynaptic tracing from single, genetically targeted neurons. Neuron. 2007; 53:639–647. [PubMed: 17329205]
17. Sheng M, Greenberg ME. The regulation and function of c-fos and other immediate early genes in the nervous system. Neuron. 1990; 4:477–485. [PubMed: 1969743]
18. McCall JG, et al. CRH engagement of the locus coeruleus noradrenergic system mediates stress-induced anxiety. Neuron. 2015; 87:605–620. [PubMed: 26212712]
19. Guyenet PG, Koshiya N, Huangfu D, Verberne AJ, Riley TA. Central respiratory control of A5 and A6 pontine noradrenergic neurons. Am J Physiol. 1993; 264:R1034–1044.
20. Oyamada Y, Ballantyne D, Mückenhoff K, Scheid P. Respiration-modulated membrane potential and chemosensitivity of locus coeruleus neurones in the in vitro brainstem-spinal cord of the neonatal rat. J Physiol. 1998; 513:381–398. [PubMed: 9806990]
21. Chen Z, Eldridge FL, Wagner PG. Respiratory-associated rhythmic firing of midbrain neurones in cats: relation to level of respiratory drive. J Physiol. 1991; 437:305–325. [PubMed: 1890637]
22. Hilaire G, Viemari JC, Coulon P, Simonneau M, Bevengut M. Modulation of the respiratory rhythm generator by the pontine noradrenergic A5 and A6 groups in rodents. Resp Physiol Neurobiol. 2004; 143:187–197.
23. Gleeson K, Zwillich CW. Adenosine stimulation, ventilation, and arousal from sleep. Am Rev Respir Dis. 1992; 145:453–457. [PubMed: 1736756]
24. Kinney HC, Thach BT. The sudden infant death syndrome. N Engl J Med. 2009; 361:795–805. [PubMed: 19692691]
25. Ramirez JM. The integrative role of the sigh in psychology, physiology, pathology, and neurobiology. Prog Brain Res. 2014; 209:91–129. [PubMed: 24746045]
26. Valença M, et al. Clonidine in respiratory panic disorder subtype. Arq Neuropsiquiatr. 2004; 62:396–398. [PubMed: 15273833]
27. Jiang M, Griff ER, Ennis M, Zimmer LA, Shipley MT. Activation of locus coeruleus enhances the responses of olfactory bulb mitral cells to weak olfactory nerve input. J Neurosci. 1996; 16:6319–6329. [PubMed: 8815911]
28. Hickey L, et al. Optoactivation of locus coeruleus neurons evokes bidirectional changes in thermal nociception in rats. J Neurosci. 2014; 34:4148–4160. [PubMed: 24647936]
29. Bielle F, et al. Multiple origins of Cajal-Retzius cells at the borders of the developing pallidum. Nature Neuroscience. 2005; 8:1002–1012. [PubMed: 16041369]
30. Gong S, et al. Targeting Cre recombinase to specific neuron populations with bacterial artificial chromosome constructs. Journal of Neuroscience. 2007; 27:9817–9823. [PubMed: 17855595]
31. Shaner NC, et al. Improved monomeric red, orange and yellow fluorescent proteins derived from Discosoma sp. red fluorescent protein. Nature Biotechnol. 2004; 22:1567–1572. [PubMed: 15558047]
32. Muzumdar MD, Tasic B, Miyamichi K, Li L, Luo L. A global double-fluorescent cre reporter mouse. Genesis. 2007; 45:593–605. [PubMed: 17868096]
33. Saito M, et al. Diphtheria toxin receptor-mediated conditional and targeted cell ablation in transgenic mice. Nature Biotechnol. 2001; 19:746–750. [PubMed: 11479567]
34. Osoegawa K, et al. Bacterial artificial chromosome libraries for mouse sequencing and functional analysis. Genome Research. 2000; 10:116–128. [PubMed: 10645956]

35. Schwarz LA, et al. Viral-genetic tracing of the input–output organization of a central noradrenaline circuit. Nature. 2015; 524:88–92. [PubMed: 26131933]

36. Osakada F, Callaway EM. Design and generation of recombinant rabies virus vectors. Nat Protoc. 2013; 8:1583–1601. [PubMed: 23887178]

37. Kremer EJ, Boutin S, Chillon M, Danos O. Canine adenovirus vectors: an alternative for adenovirus-mediated gene transfer. Journal of Virology. 2000; 74:505–512. [PubMed: 10590140]

38. Schoenenberger P, Gerosa D, Oertner TG. Temporal control of immediate early gene induction by light. PLoS One. 2009; 4:e8185. [PubMed: 19997631]

39. Luckman SM, Dyball RE, Leng G. Induction of c-fos expression in hypothalamic magnocellular neurons requires synaptic activation and not simply increased spike activity. Journal of Neuroscience. 1994; 14:4825–4830. [PubMed: 8046453]

40. Peng H, Bria A, Zhou Z, Iannello G, Long F. Extensible visualization and analysis for multidimensional images using Vaa3D. Nature Protocols. 2014; 9:193–208. [PubMed: 24385149]

41. Kreuzer M, et al. Sleep scoring made easy-semi-automated sleep analysis software and manual rescoring tools for basic sleep research in mice. MethodsX. 2015; 24:232–240.

42. Karasinski P, Stinus L, Robert C, Limoge A. Real-time sleep-wake scoring in the rat using a single EEG channel. Sleep. 1994; 17:113–119. [PubMed: 8036365]

43. Schofield BR. Retrograde axonal tracing with fluorescent makers. Curr Protoc Neurosci. 2008; Chapter 1(Unit 1.17)

44. Callaway EM, Luo L. Monosynaptic circuit tracing with glycoprotein-deleted rabies viruses. Journal of Neuroscience. 2015; 35:8979–8985. [PubMed: 26085623]

45. Kam K, Worrell JW, Janczewski WA, Cui Y, Feldman JL. Distinct inspiratory rhythm and pattern generating mechanisms in the preBötzinger complex. J Neurosci. 2013; (33):9235–9245. [PubMed: 23719793]

46. Hama H, et al. Scale: a chemical approach for fluorescence imaging and reconstruction of transparent mouse brain. Nature Neuroscience. 2011; (14):1481–1488. [PubMed: 21878933]

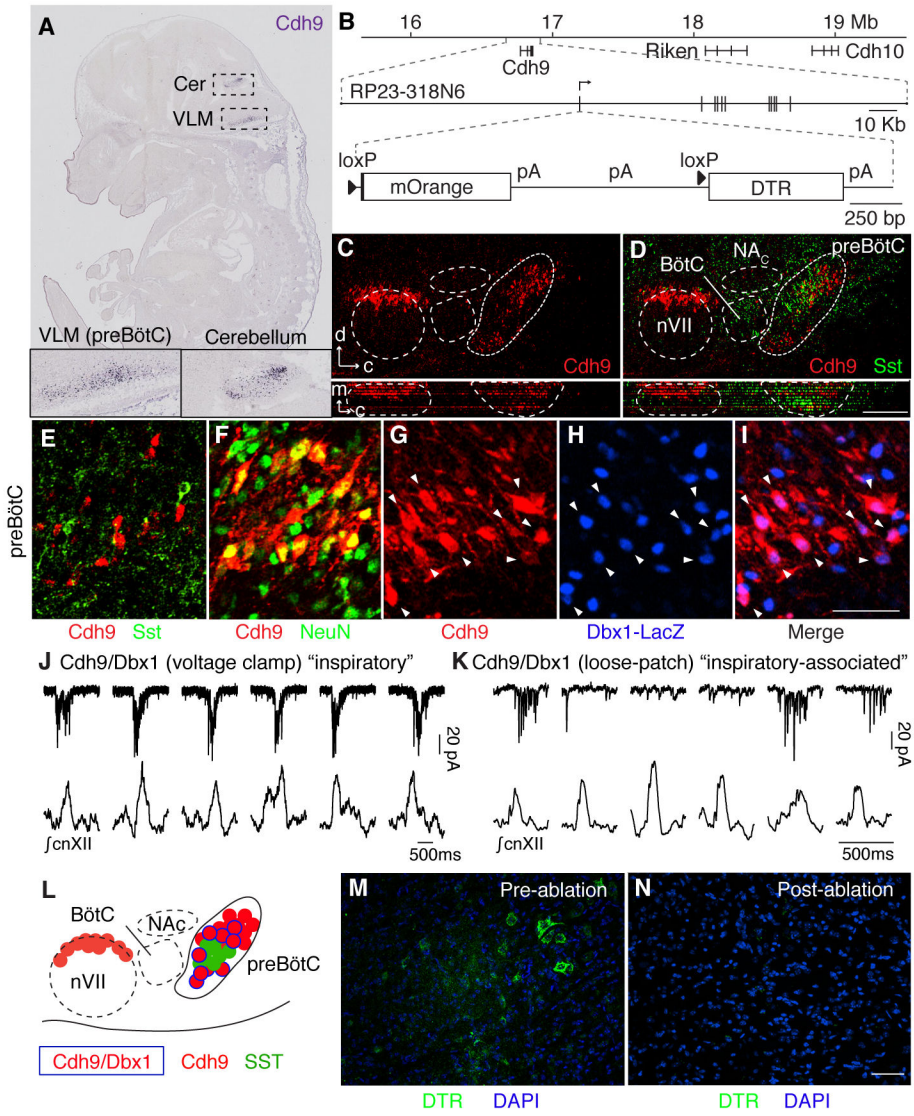

Fig. 1. Identification and genetic ablation of Cdh9/Dbx1 double positive neurons in preBötC

A, *Cdh9* mRNA expression (blue) in section of E14.5 mouse embryo (11). Insets, ventrolateral medulla, ventral cerebellum. **B**, (Top) *Cdh9* locus on chromosome 15 (numbers, distance from centromere). (Middle) BAC RP23-318N6. Vertical lines, *Cdh9* exons. (Bottom) Cdh9-LOSL-DTR BAC transgene: insertion at Cdh9 start codon of mOrange sequence and polyadenylation (pA) signals, flanked by *loxP* sites (triangles), followed by DTR sequence. **C,D**, Ventrolateral medulla sections of P0 Cdh9-LOSL-DTR mouse immunostained for mOrange to show Cdh9 expression (red) and P0 wild type mouse immunostained for Somatostatin (SST, green), shown aligned (registered by compact nucleus ambiguus (NA_C), cranial nerve 7 (nVII), and ventral brainstem surface) in sagittal plane (upper) and transverse projection (lower panels). d, dorsal; c, caudal; m, medial. Bar, 200 μm. **E–I,** preBötC of P0 Cdh9 LOSL-DTR (E,F) or Cdh9-LOSL-DTR;Dbx1-lacZ (G–I) mouse immunostained for Cdh9-mOrange (E–G,I, red), SST (E, green), NeuN (F, green) or beta-galactosidase (Dbx1-LacZ, H,I, blue). Among Cdh9-neurons, none co-expressed SST

(n=43 cells), all co-expressed NeuN (n=57), and 56% co-expressed Dbx1 reporter (n=292, arrowheads). Bar (for E–I), 50 μm. **J,K,** Whole cell voltage clamp recordings (top, pA, picoAmp) of Cdh9/Dbx1 preBötC neurons in slice preparations (top) and simultaneous integrated cnXII activity (bottom). Neuron in J (neuron 1, Table S1) shows bursts in all inspiratory events ("inspiratory pattern"). Neuron in K (neuron 3) shows more widespread activity but bursts only during some events ("inspiratory-associated"). Bars, 500 msec. **L**, Schematic of ventrolateral medulla. Cdh9/Dbx1 neurons (blue border) intermingle with SST (green) and other Cdh9 neurons (red) in preBötC. **M,N**, Intersectional genetic labeling of Cdh9/Dbx1 preBötC neurons with DTR (immunostain, green) in ~P35 Cdh9-LOSL-DTR;Dbx1-cre mice before (M) and after (N) intraperitoneal DT injection to ablate them. Bar, 50 μm.

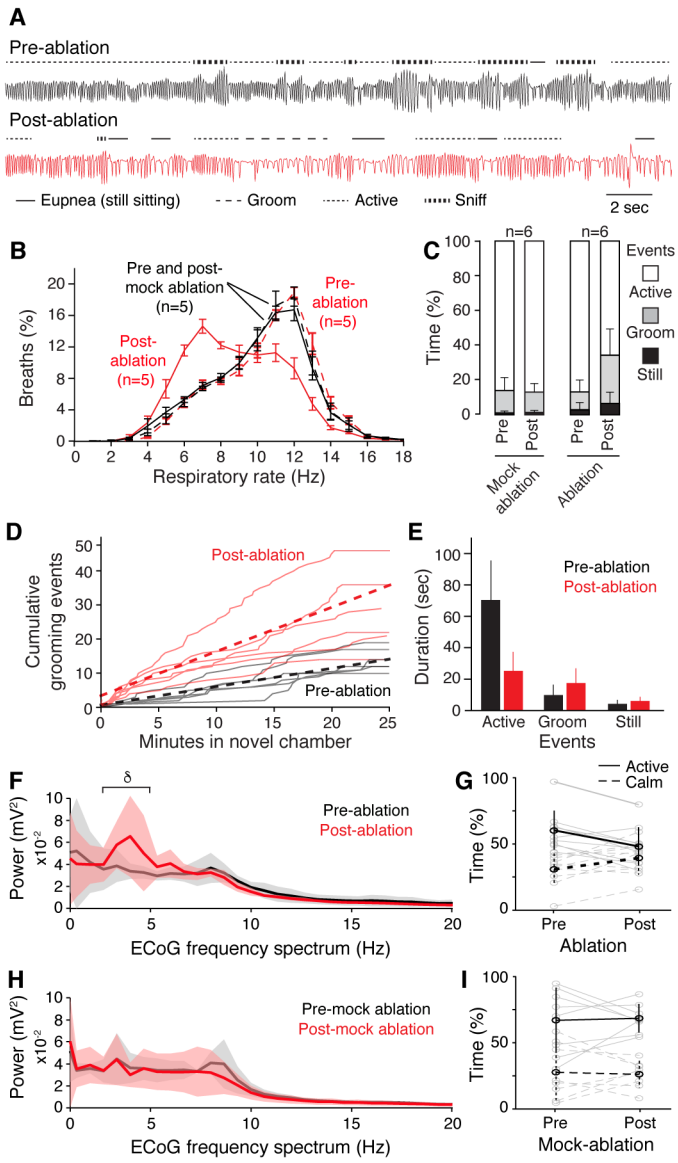

Fig. 2. Respiratory and behavior changes after Cdh9/Dbx1 neuron ablation

A, Plethysmography airflow traces of Cdh9-LOSL-DTR;Dbx1-Cre mice before (black) and 2 days after (red) Cdh9/Dbx1 ablation. Note more grooming (− −) and eupneic (−) breaths and less active breaths (− −) and sniffing (−−) after ablation. Bar, 2 seconds. **B,** Distribution of respiratory rates (Hz, bin size 1 Hz) in 40 minute assay of control (wild type, Cdh9-LOSL-DTR or Dbx1-Cre; black, n=5) and experimental (Cdh9-LOSL-DTR;Dbx1-Cre; red, n=5) animals before (dashed lines) and 2 days after (solid lines) Cdh9/Dbx1 ablation. **C**, Percent of time in plethysmography chamber spent still sitting (black), grooming (grey) or active (white) by control (n=6) or experimental (n=6) mice before (pre) or 2 days after (post) ablation or mock ablation. p-value comparing pre- and post-ablation behavior: active (0.02), grooming (0.02), still sitting (0.07). **D,** Grooming events in new chamber of Cdh9-LOSL-DTR;Dbx1-Cre mice before (black) or after (red) ablation. Solid lines, individual mice (n=6); dotted line, average. **E,** Duration of behaviors in C (mean ± S.D., n = 6). After

ablation, active episodes shortened (p = 0.005), grooming and still sitting showed non-significant trend to lengthening (p=0.24 and 0.21, respectively). **F,H,** ECoG power spectral analysis (average (solid lines) ± S.E.M) of 20-minute recording (trial 1) of Cdh9-LOSL-DTR;Dbx1-Cre (F, n = 5) or control Cdh9-LOSL-DTR (H, n = 4) mice before (black) or 4–10 days after (red) ablation. **δ**, delta wave. V, voltage. Active behavior correlates with faster breathing (fig. S15C–E). **G,I,** Time spent in active (solid black line, mean ± S.E.M) and calm (dashed black line) behavioral states defined by EMG and ECoG (fig. S15) of individual animals in F,H (gray lines) during two 20-minute assays pre- and post-Cdh9/Dbx1 ablation. Note decreased active and increased calm periods following ablation in experimental animals (p = 0.001 and 0.02, respectively, paired t-test) and no change in controls (p = 0.86 and 0.81, respectively).

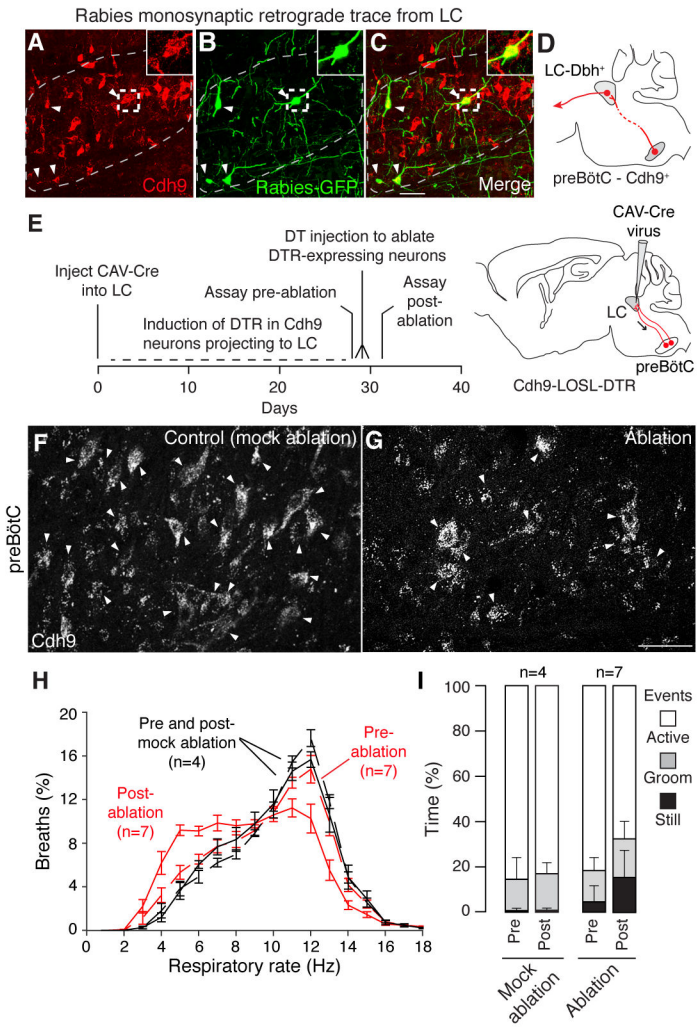

Fig. 3. Effect on breathing and behavior of ablation of Cdh9 neurons that project to and synapse on LC neurons

A–D, Rabies virus monosynaptic retrograde trace from dopamine beta hydroxylase (Dbh)-expressing locus coeruleus (LC) neurons. Section through contralateral preBötC (A–C) of adult Cdh9-LOSL-DTR;Dbh-Cre mouse 5 days after unilateral LC injection of rabies-GFP and helper virus, immunostained to show Cdh9 neurons (mOrange, red). Arrowheads, colocalization of GFP and mOrange. Insets, boxed regions. Bar, 50 μm. **D**, Schematic of monosynaptic projection (red line) from Cdh9 preBötC neurons (red circle) to contralateral LC, which projects to higher brain structures (arrow). **E,** Scheme for ablating only Cdh9-expressing preBötC neurons that project to LC. CAV-Cre virus injected bilaterally into LC of adult Cdh9-LOSL-DTR mice (right) is taken up by Cdh9 preBötC neurons that project there (red). Cre induces DTR expression, and DT injection induces ablation. **F–G,** preBötC Cdh9-mOrange expression (white) in control uninjected (F, mock ablation) and CAV-Cre injected (G, ablation) Cdh9-LOSL-DTR mice 2 days after DT injection. Bar, 50 μm. Quantification showed 32% (mean) and 50% (maximal) reduction in mOrange neurons (n = 15 sections), close to the value expected if all Cdh9/Dbx1 preBötC neurons (50% of Cdh9 neurons) project to LC. **H**, Distribution of respiratory rates in 40 min assay (as in Fig. 2B) of CAV-

Cre injected Cdh9-LOSL-DTR adult mice (red, n = 7) or wild type littermates (black, n = 4) before (dashed) and 2 days after (solid) DT injection. **I**, Behavioral analysis (as in Fig. 2C) of mice in H. Pre vs. post-ablation p-values: active (0.015), grooming (0.37), and still sitting (0.015). The increased calm events in pre-ablation experimental versus control mice was reproducible; it may be due to toxicity of DTR induced in adult neurons, which curiously is not observed in Cdh9-LOSL-DTR;Dbx1-Cre mice when DTR is expressed in early development, perhaps due to developmental compensation.

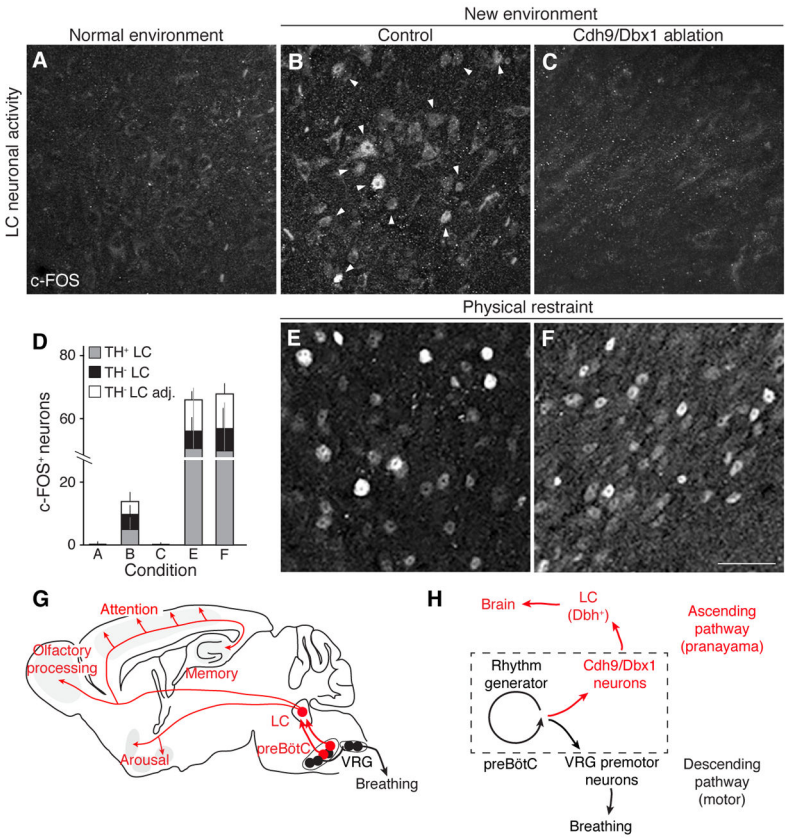

Fig. 4. Effect of Cdh9/Dbx1 neuron ablation on LC neuronal activity

A–C, E–F, c-FOS immunostaining (arrowheads) in LC of adult wild type mouse in normal environment (home cage, A) and of control (wild type, Cdh9-LOSL-DTR, or Dbx1-Cre mice, B,E) and Cdh9/Dbx1-ablated mice (Cdh9-LOSL-DTR;Dbx1-cre mice 2 days after DT injection, C,F) after 1 hour in new chamber (B,C) or in a conical tube under physical restraint (E,F). Bar, 50 μm. **D**, Quantification of c-FOS$^+$ neurons in A–C and E–F (mean ± SD) per 25 μm section of LC: A, 0.4 ± 0.8 neurons (n = 39 sections, 6 animals); B, 13.8 ± 6.5 neurons (14 sections, 4 animals); C, 0.1 ± 0.3 neurons (17 sections, 6 animals); E, 61.4 ± 31.4 neurons (5 sections, 3 animals); F, 63.8.8 ± 19.9 neurons (6 sections, 3 animals). c-FOS$^+$/TH$^+$ neurons, gray; c-FOS$^+$/TH$^-$ neurons embedded within TH$^+$, black; c-FOS$^+$/TH$^-$ neurons directly surrounding TH$^+$ LC region, white. **G,** Ascending neural circuit from preBötC. Cdh9/Dbx1 preBötC neurons (red) provide monosynaptic excitatory input to noradrenergic locus coeruleus (LC) neurons (red), which project throughout brain to promote arousal and active behaviors. Also shown is the classical circuit from preBötC rhythm-generating neurons (black) to premotoneurons in ventral respiratory group (VRG, black). **H,** Model of preBötC with Cdh9/Dbx1 neurons distinct from, but regulated by rhythm generating neurons. This provides an ascending respiratory corollary signal to LC on to rest of brain, separate from classical descending motor circuit. Hence, when breathing speeds up or is otherwise altered, Cdh9/Dbx1 neurons activate LC to induce or maintain an aroused state. (Less direct circuits or downstream events from Cdh9/Dbx1 neurons could also contribute to LC activation, and because LC also regulates sensory modalities (27, 28),

sensory alterations could also contribute to LC-induced behaviors. Also, a direct contribution of Cdh9/Dbx1 neurons to preBötC breathing rhythm generation cannot be excluded, because compensatory mechanisms may obscure them.)